NIST Technical Note 1940

Database-Assisted Design and second-order effects on the wind-induced structural behavior of high-rise steel buildings

Sejun Park
DongHun Yeo

This publication is available free of charge from:
https://doi.org/10.6028/NIST.TN.1940

National Institute of
Standards and Technology
U.S. Department of Commerce

NIST Technical Note 1940

Database-Assisted Design and second-order effects on the wind-induced structural behavior of high-rise steel buildings

Sejun Park
DongHun Yeo
Engineering Laboratory
National Institute of Standards and Technology
Gaithersburg, MD 20899-7311

This publication is available free of charge from:
https://doi.org/10.6028/NIST.TN.1940

October 2016
Includes updates as of 03-07-2017; See Appendix 3

U.S. Department of Commerce
Penny Pritzker, Secretary

National Institute of Standards and Technology
Willie May, Under Secretary of Commerce for Standards and Technology and Director

National Institute of Standards and Technology Technical Note 1940
Natl. Inst. Stand. Technol. Tech. Note 1940, 37 pages (October 2016)
CODEN: NTNOEF

This publication is available free of charge from:
https://doi.org/10.6028/NIST.TN.1940

Disclaimers

(1) The policy of the NIST is to use the International System of Units in its technical communications. In this document however, works of authors outside NIST are cited which describe measurements in certain non-SI units. Thus, it is more practical to include the non-SI unit measurements from these references.

(2) Certain trade names or company products or procedures may be mentioned in the text to specify adequately the experimental procedure or equipment used. In no case does such identification imply recommendation or endorsement by the National Institute of Standards and Technology, nor does it imply that the products or procedures are the best available for the purpose.

Abstract

This work presents an investigation into second-order effects on the wind-induced structural dynamic behavior of high-rise steel structure, as considered within a Database-assisted Design (DAD) context. A geometric stiffness method that accounts for second-order effects and allows the dynamic analysis to be performed without iterations is shown to be applicable in conjunction with DAD and is used in a study of the response of a 60-story building, known as the CAARC building. Datasets of the aerodynamic pressure on the CAARC building for suburban exposure are used to calculate overturning moments and shear forces at the base, as well as members' demand-to-capacity indexes (DCIs), inter-story drift ratios, and resultant accelerations. Dynamic analyses are performed using five reference mean hourly wind speeds at the rooftop for suburban terrain exposure (U_{ref} = 20 m/s, 40 m/s, 60 m/s, 80 m/s, and 100 m/s). The first three and the last three wind speeds are used in analyses for serviceability and strength, respectively. The second-order effects decrease natural frequencies of vibration of the building by up to 12 %. If the resonant response is not taken into account and for $U_{ref\,=}$ 80 m/s, second-order effects increase the non-directional peak base shears by up to 9 %, the torsional moments by up to 10 %, and the overturning moments by up to 15 %. If resonance is accounted for, (i) for U_{ref} = 100 m/s normal to a building face, the vortex shedding frequency is close to the 2nd and the 3rd natural frequencies of the building, and those effects are increased by 40 % to 56 %; for U_{ref} = 80 m/s and a typical set of 21 structural members, the DCIs for the interaction of axial forces and bending moments, $B_{ij}{}^{PM}$, are increased by up to 19 % for columns, 41 % for beams, and 31 % for diagonal bracings, while the DCIs for the shear forces, $B_{ij}{}^{V}$ are increased by up to 67 % for columns, 26 % for beams, and 13 % for diagonal bracings; (iii) for U_{ref} = 60 m/s, second-order effects increase the inter-story drift ratios by up to 40 % and the resultant accelerations at the top floor by up to 20 %.

Keywords: CAARC building; Database-Assisted Design (DAD); Demand-to-capacity index (DCI); Geometric stiffness approach; High-rise steel structures; Second-order effects; Wind effects.

Acknowledgement

The wind tunnel data developed at the CRIACIV-DIC Boundary Layer Wind Tunnel were kindly provided by Dr. Ilaria Venanzi of the University of Perugia. Dr. Emil Simiu served as project leader and provided helpful comments, and careful review by Dr. John Gross of National Institute of Standards and Technology is acknowledged with thanks.

Contents

List of Figures

List of Tables

1. Introduction

In high-rise buildings gravity loads cause an amplification of the structural system's displacements and moments induced by lateral loads. The amplification is a second-order effect that includes both the P-Δ effect due to member chord rotation and the P-δ effect due to member curvature. High-rise buildings, which typically have fundamental frequencies of vibration lower than 1 Hz, tend to be more susceptible to second-order effects associated with wind than with seismic loads, since wind loads are generally characterized by low frequencies while seismic loads usually have higher frequency content. Therefore, controlling second-order effects of high-rise buildings subjected to the wind loading is necessary from a perspective of both strength design and serviceability. Two basic approaches to assessing dynamic instability induced by secondary effects on multi-story buildings have been developed to date: (1) second-order elastic analysis with geometric nonlinearities and (2) second-order inelastic analysis with geometric and material nonlinearities.

Within the framework of the second-order elastic analysis, several methods have been proposed. The additional story shear force method, which deals only with the P-Δ effect approximately, implements additional story shears due to the vertical loads with regard to the deformed geometry of the structure, and subsequent reanalysis should be performed iteratively (Wood et al. 1976). The moment amplification method (also known as *B1*/*B2* approach introduced in ANSI/AISC 2010a and LeMessurier 1976, 1977), which involves the calculation of B1 (for P-δ) and B2 (for P-Δ), is simple and fast, and is for this reason commonly used in design practice. However, the approximations it entails may be unsatisfactory in some cases. The fictitious column method proposed by Rutenberg (1981) considers the secondary effect by using a fictitious member having negative lateral stiffness properties proportional to the story weights. This fictitious member reduces the lateral stiffness of the structure so that the drifts and moments of members can be functions of the lateral loads and of the gravity loads. The method requires no iterations and only slightly underestimates the secondary effects even when the P-δ effect is not included. As computational capabilities have advanced, matrix analysis approaches have been developed. These approaches can accurately account for both P-Δ and P-δ effects by employing stability functions (Goto and Chen 1987) or geometric stiffness formulations (Wilson and Habibullah 1987). If stability functions are used, the governing differential equations of a beam-column element are solved iteratively by updating the stiffness matrix and the force vector due to the secondary effects (Al-Mashary and Chen 1990). In the geometric stiffness formulation, an assumed cubic polynomial shape function is employed to solve the governing equations; this is computationally more advantageous than the use of stability functions.

Among second-order inelastic analyses, the pushover analysis have been widely used. For simplicity, the inelastic material behavior is typically assumed to be bilinear with zero post-yield stiffness (i.e., elastic-perfectly plastic). Several nonlinear dynamic analysis techniques for multi- or equivalent single-degree-of-freedom systems are then applied to estimate the inelastic dynamic responses. Bernal (1998), MacRae (1993), Tremblay et al. (2001), Gupta and Krawinkler (2000), and Humar et al. (2006) carried out inelastic dynamic analyses on various models of multi-story buildings designed for seismic loads and proposed several methods of accounting for the secondary effects. They reported that the second-order effects typically result in an increase of the response over the first-order response by approximately 10 % to 25 %, depending upon the lateral forces resisting system, the number of stories, and the magnitude and duration of ground motions.

Second-order effects on tall buildings have been extensively investigated for the case of seismic loads (Gupta and Krawinkler 2000; Humar et al. 2006; MacRae 1993; Williamson 2003). However, research for the case of wind loads has been much more limited. The ASCE task committee on drift control of steel building structures has suggested such research (ASCE 1988). Analytical studies have, therefore, been performed on steel frames subjected to wind to assess second-order effects on lateral drift of structures as they affect serviceability (Baji et al. 2012; Berding 2006). However, these studies did not include second-order effects on structural strength.

The main objective of this report is to study the second-order effects on the wind-induced strength and serviceability behavior of a high-rise steel structure. This study adopted the geometric stiffness approach and, as shown in Section 2, used this approach in conjunction with the Database-Assisted Design (DAD) technique to account for secondary effects on dynamic structural responses under wind with various speeds and directions. The structural system was assumed to behave linearly (i.e., material nonlinearity is not considered). In Section 3 that approach was applied to a 60-story building, known as the CAARC building model, in suburban exposure, for which the wind load was based on aerodynamic pressure datasets obtained in wind tunnel tests. First- and second-order responses were evaluated for overturning moments and base shear forces, members' demand-to-capacity indexes (DCIs), inter-story drift ratios, and accelerations. A section on conclusions ends this work.

2. The use of the DAD procedure for the evaluation of second-order effects

2.1. Geometric stiffness approach for second-order elastic analysis

In second-order elastic analyses of both P-Δ (member chord rotation effects) and P-δ (member curvature effects), static equilibrium is formulated on the deformed configuration of the structure. The secondary effects can be accounted for by using a matrix known as the geometric stiffness matrix [also called initial stress stiffness matrix, Wilson and Habibullah (1987)]. For the frame analysis, the geometric stiffness matrix represents the stiffening and weakening effect by the tensile (positive) and compressive (negative) load in the structural member, respectively. The method does not require iterations. The second-order problem can be formulated and solved as a linear system where the geometric stiffness matrix is subtracted from the elastic stiffness matrix, as expressed in Eqs. 1 to 3. The following example is an application to a two-dimensional beam element with six degrees of freedom (Chen and Lui 1987):

$$F = [K - K_G] \cdot \Delta \tag{1}$$

$$[K] = \frac{EI}{L} \cdot \begin{bmatrix} A/I & 0 & 0 & -A/I & 0 & 0 \\ & 12/L^2 & 6/L & 0 & -12/L^2 & 6/L \\ & & 4 & 0 & -6/L & 2 \\ & & & A/I & 0 & 0 \\ & sym. & & & 12/L^2 & -6/L \\ & & & & & 4 \end{bmatrix} \tag{2}$$

$$[K_G] = P \cdot \begin{bmatrix} 0 & 0 & 0 & 0 & 0 & 0 \\ & 6/5L & 1/10 & 0 & -6/5L & 1/10 \\ & & 2L/15 & 0 & -1/10 & -L/30 \\ & & & 0 & 0 & 0 \\ & sym. & & & 6/5L & -1/10 \\ & & & & & 2L/15 \end{bmatrix} \tag{3}$$

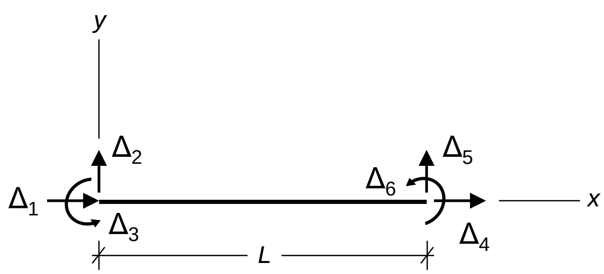

Figure 1. Degrees of freedom of 2D beam-column element

where F is the applied static lateral force matrix; K is the elastic stiffness matrix; Δ is the element nodal displacement vector; K_G is the geometric stiffness matrix, which accounts for second-order moments caused by the interaction of the gravity loads (P) and the lateral deflections of structure; L is the element length; E is the modulus of elasticity; A and I are the cross-sectional area and the inertia moment of the member, respectively (Figure 1).

In the geometric stiffness method, (1) if the initial axial forces in the elements are significantly modified by the application of external loads, iterative calculations may be required, and (2) if P/P_e exceeds 0.4, where $P_e = \pi^2 EI/L^2$, the corresponding members must be subdivided into two or more elements to limit the errors in the stiffness matrix; this is associated only with the P-δ amplification (White and Hajjar 1991). This solution is as accurate as the exact solution obtained by a matrix approach based on stability functions (Al-Mashary and Chen 1990).

The matrix equation of dynamic equilibrium in a structural system is:

$$M\ddot{\Delta}(t) + C\dot{\Delta}(t) + [K - K_G]\Delta(t) = F(t) \tag{4}$$

where M, C, and $F(t)$ are the mass, damping, and external excitation matrix at time t, respectively. Since the lateral stiffness of the structural system is effectively reduced by K_G, the natural frequencies of vibration will be lowered and the modal shapes will be slightly changed in comparison with those of the analysis in which secondary effects are not accounted for. These lower frequencies and the corresponding modal shapes represent the actual free vibration responses of the structure (Newmark and Rosenblueth 1971). Based on the dynamic properties resulting from Eq. 4, the DAD procedure can be used to evaluate the structural response to wind and perform the design procedure for a high-rise building by considering the second-order effects under wind excitation.

2.2. Overview of the DAD procedure

Figure 2 illustrates the DAD procedure for the case in which second-order effects on a high-rise building are considered. The procedure within the dotted lines box represents the main algorithm of the High-Rise Database-Assisted Design (HR_DAD_2.0) software. The software HR_DAD_2.0 is similar to the software HR_DAD_RC developed by Yeo (2010), with an additional function that accounts for second-order effects. The natural frequencies of vibration and mode shapes can then be obtained by a modal analysis that employs a finite-element analysis program, and are input into the main DAD algorithm described in Fig. 2. In the modal analysis the factored dead and live loads should be used as vertical loads (White and Hajjar 1991). A separate second order analysis is required for each factored load combination (as shown in Eqs. 5 and 6). In the DAD module, dynamic analyses are performed for the building model with a lumped mass, gravity load and a wind load on each floor. The wind loads applied at the floors' mass centers are calculated from aerodynamic pressures on the building for five wind speeds and a sufficiently large set of wind directions. The outputs of the dynamic analyses consist of (1) sums of time-series of the aerodynamic and inertial forces applied at the center of mass in the direction of each of the two principal axes of the building, as well as of the sum of the aerodynamic moment and inertial moment about the center of mass. (2) time-series of displacements and accelerations at each floor level. These results are converted, for example, through the use of influence coefficients, into time-series of internal forces, and time-series of demand-to-capacity indexes (DCIs) for each structural member of interest, as well time-series of inter-story drifts in the principal directions of the structure along column lines, and resultant accelerations at corners of the top floor.

It is recalled that the DCI of a structural member is the left-hand side of the design interaction equation. Details on the DCIs employed in this study are provided in Appendix 1. For design purposes, the peak of the time-series of each DCI is used and can be efficiently calculated using the multiple points-in-time (MPIT) approach (Yeo 2013). This study uses 30 peaks of individual wind effects (Yeo and Simiu 2011). Directional wind effects are calculated by using directional wind speed climatological databases (hurricane and/or non-hurricane datasets). The peak wind effects with a specified Mean Recurrence Interval (MRI) of, e.g., 700 years or 1700 years, are estimated using a non-parametric statistical method (for details see Section 12.4 in Simiu 2011).

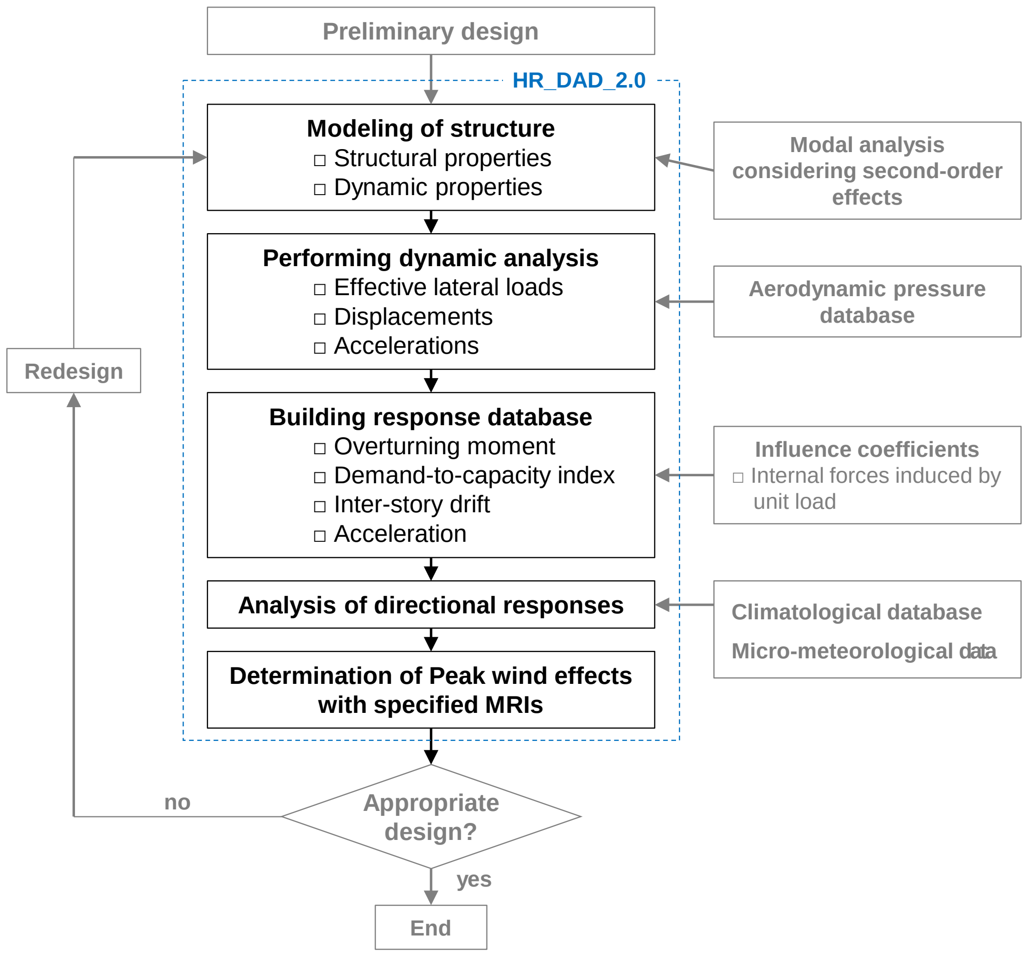

Figure 2. Overview of DAD procedure

3. Case study

Figure 3 depicts the 60-story high-rise steel structure being considered, with 182.88 m height, 45.72 m width, and 30.48 m depth, known as the CAARC (Commonwealth Advisory Aeronautical Research Council) building, studied by various researchers (Melbourne 1980; Simiu et al. 2008; Venanzi 2005). Wind direction is defined by the clockwise angle θ, with the positive x-axis parallel to the long dimension, and the y-axis parallel to the short dimension of the building cross section. The building has an outrigger system to resist the lateral load similar to the structural system studied by Simiu et al. (2008) and consists of 2,100 columns, 3,480 beams, and 2,560 diagonal bracings. Columns and beams are classified into three types as corner, external, and core for columns, and external, internal, and core for beams, respectively. Diagonal bracings are divided into two types as core and outrigger bracings. Each type of structural member (column, beam, bracing member) has the same dimensions for ten successive floors of the building's 60 floors. The columns and bracings consist of built-up hollow structural sections (HSS), and the beams consist of rolled W-sections selected from the Steel Construction Manual of

AISC (ANSI/AISC 2010b). The yield strength of steel for all members is 250 MPa. The modal damping ratios were assumed to be 1.5 % in all modes considered in this study.

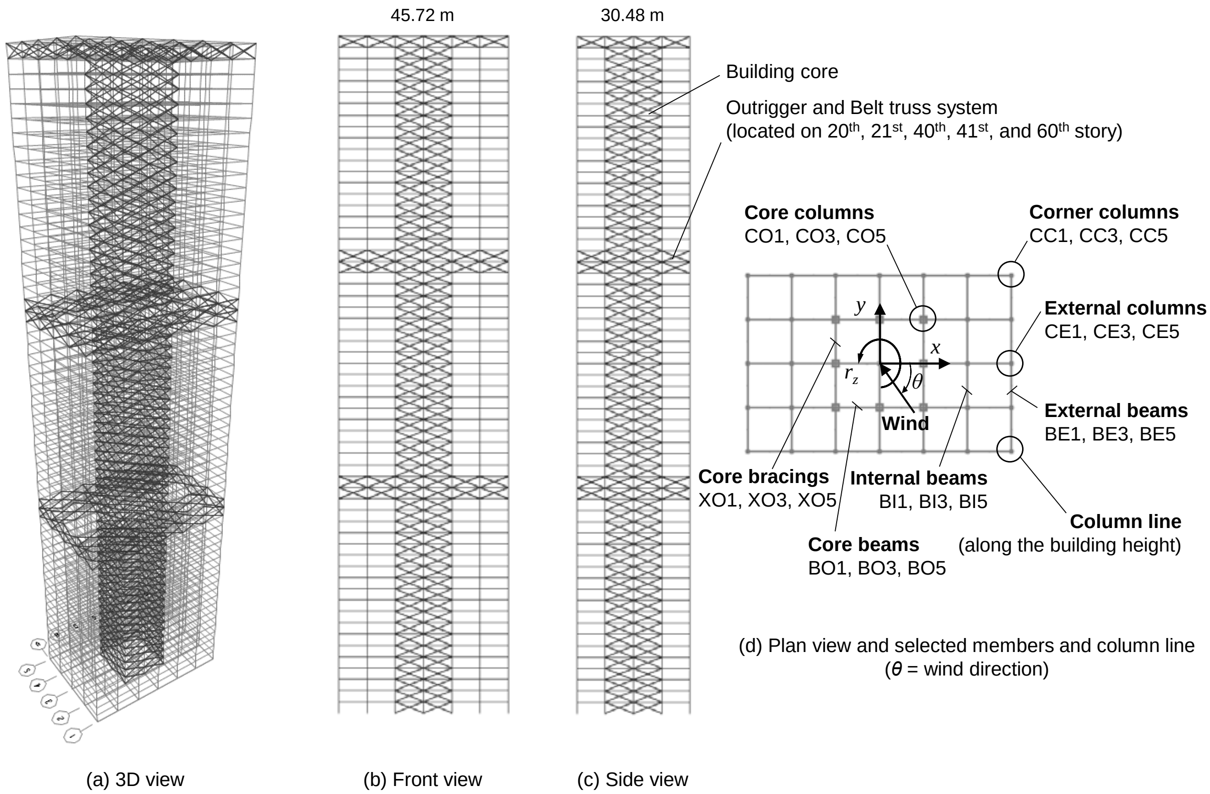

Figure 3. Schematic views of structural system and selected members

The building was assumed to have suburban terrain exposure. Time series of aerodynamic loads on each floor were calculated from the pressure data, with wind directions in 10° increments measured in wind tunnel experiments at the Prato (Italy) Inter-University Research Centre on Building Aerodynamics and Wind Engineering (CRIAC IV-DIC) Boundary Layer Wind Tunnel (Venanzi 2005).

Under the assumption of linear elastic structural behavior, dynamic analyses of the building were carried out for serviceability and strength. Load combinations associated with gravity and wind loads with MRIs specified by ASCE 7-10 (ASCE 2010). Two load combination cases (LC1 and LC2 in Eq. 5) were employed for strength design (Section 2.3 in ASCE 2010) and one (LC3 in Eq. 6) was employed for serviceability design (see Commentary Appendix C in ASCE 2010):

$$1.2D + 1.0L + 1.0W \text{ (LC1)} \quad \text{and} \quad 0.9D + 1.0W \text{ (LC2)} \tag{5}$$

$$1.0D + 0.5L + 1.0W \text{ (LC3)} \tag{6}$$

where D is the dead loads, L is the live loads, and W is the wind loads, respectively.

3.1. Dynamic properties and modal contribution

Once initial dimensions of members in the building were obtained, the modal analysis was conducted with and without the second-order effects to calculate the respective natural frequencies and mode shapes using SAP 2000 v.17 (Computers and Structures Inc. 2015). Figure 4 and Table 1 show the mode shapes and the corresponding natural frequencies up to the 6th mode, respectively. The first mode corresponds to drift along the *y*-axis, the second to drift along the *x*-axis, the third to rotation along the *z*-axis. The following fourth, fifth, and sixth modes correspond to the second mode of the *y*-dir. translational motion, the rotational motion, and the *x*-dir. translational motion, respectively. As shown in Table 1, the second-order effects decrease the natural frequencies of the building by up to 12 %. As a result, the frequencies of the 2nd and the 3rd modes become 0.164 Hz and 0.165 Hz, which differ by less than 1%.

For the investigation of modal contributions to structural responses to wind, dynamic analyses by the HR_DAD_2.0 algorithm based on the modal superposition method were performed with 12 accumulated mode cases from the 1st mode up to the 12th mode (i.e., 1st, 1st – 2nd, … 1st – 12th). For example, for the resultant top-floor acceleration at a building corner, Figure 5 represents the ratios of the peak resultant accelerations with and without second-order effects in the accumulated mode cases to their counterparts without the effects in the modes up to 12th mode. The accelerations were calculated at a corner of the top-floor under mean hourly wind speed at the top floor level of 60 m/s with θ = 90°. As shown in the figure, the acceleration ratios without second-order effects are 0.74 for the first two modes, 0.93, 0.96, 0.99, and 1.00 for the first three, four, five, and six modes. A similar trend is shown in the analysis with second-order effects, except for an approximately 7 % increase of their magnitudes in comparison with the analysis without second-order effects. These results imply that it is reasonable to use the first six modes in the modal superposition analysis for accurately assessing the dynamic responses of the high-rise building model to wind considered in this study, with or without accounting for second-order effects.

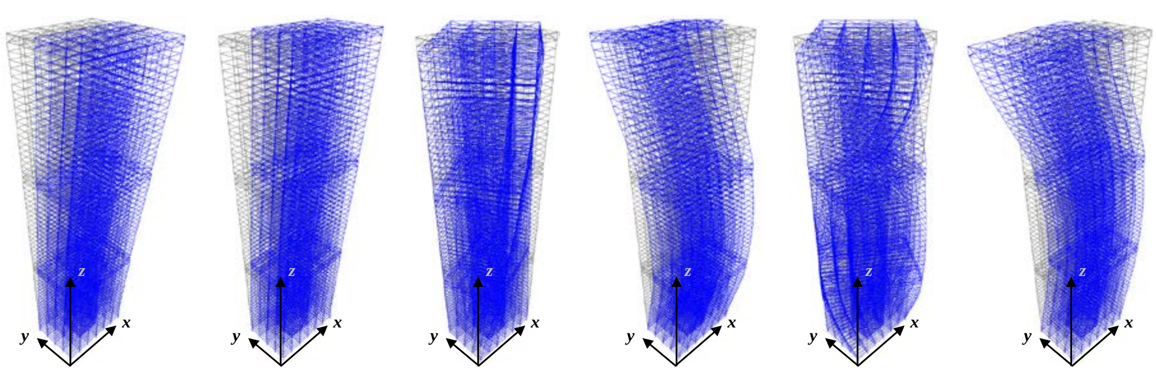

1st mode	2nd mode	3rd mode	4th mode	5th mode	6th mode
(a) 1st translational mode in y-dir.	(b) 1st translational mode in x-dir.	(c) 1st rotational mode in z-dir.	(d) 2nd translational mode in y-dir.	(e) 2nd rotational mode in z-dir.	(f) 2nd translational mode in x-dir.

Figure 4. First six mode shapes

Table 1. Dynamic properties of building with and without second-order effects

Mode		1st	2nd	3rd	4th	5th	6th
Natural freq. (Hz)	1st order (A)	0.165	0.174	0.188	0.503	0.505	0.516
	2nd order (B)	0.154	0.164	0.165	0.478	0.484	0.498
Ratio (B/A)		0.93	0.94	0.88	0.95	0.96	0.97

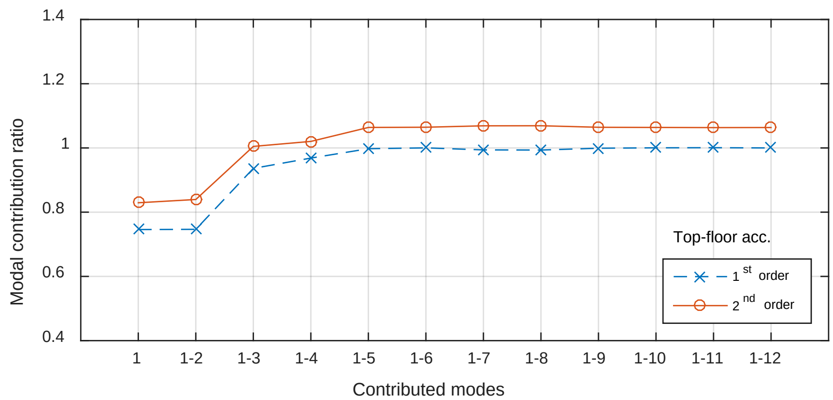

Figure 5. Accumulated modal contributions to resultant top-floor accelerations

3.2. Dynamic responses considering second-order effects

Dynamic analyses under LC1 (Eq. 5) were performed using five reference wind speeds (U_{ref} = 20 m/s, 40 m/s, 60 m/s, 80 m/s, and 100 m/s; mean hourly wind speeds at the rooftop of the building with suburban terrain exposure). Although the probability of attaining a 100 m/s wind speed is not considered in current building codes, this speed is included in this study for illustrative purposes. These wind speeds can be converted to 3-sec gust wind speeds at 10 m elevation over open terrain exposure resulting in approximately 22 m/s, 43 m/s, 65 m/s, 87 m/s, and 108 m/s, respectively. The first three wind speeds were selected for serviceability design analysis since they correspond to typical ASCE-based basic wind speeds with MRI up to 100 years (see Figures CC-1 to CC-4 in ASCE 7-10 2010), and the last three wind speeds were chosen for strength design analysis because they are as high as the basic wind speeds for Occupancy Category III and IV buildings with MRI up to 1,700 years (see Figure 26.5-1B in ASCE 7-10 2010). Note that the basic wind speed for Occupancy Category IV buildings near Miami, Florida is approximately 90 m/s corresponding to MRI = 3,000 years in the ASCE 7-16 draft (ASCE 2016). Though the wind directions considered in this study are θ = 0° to θ = 350° in increments of 10°, for reasons of symmetry only directions from θ = 0° to θ = 90° need to be used.

In the analysis of dynamic response to wind using Eq. 4, the effective force applied to the mass center of the n^{th} floor of the structure can be calculated as:

$$F_n^{eff}(t) = P_n(t) - M_n \ddot{\Delta}_n(t) - C_n \dot{\Delta}_n(t) \tag{7}$$

where the terms in the right-hand side are the forces related to wind (P_n), inertia (M_n), and damping (C_n) matrices at each n^{th} floor, respectively. Note that the damping force is negligibly small in comparison with the other forces. Figure 6 shows time histories of the wind aerodynamic loads [$P(t)$] and the effective dynamic responses (base shear) in the analyses with and without second-order effects when the wind of U_{ref} = 80 m/s approaches the building with wind direction of θ = 90° (i.e., the direction parallel to the short dimension of the building). In the plots the loads are normalized based on the absolute peak of the loads obtained in the analysis with no second-order effects. The horizontal solid lines represent positive or negative peak loads with second-order effects. It is seen that the across-wind response with the second-order effects is larger than that without the effects while the second-order effect is not significant for the along-wind response.

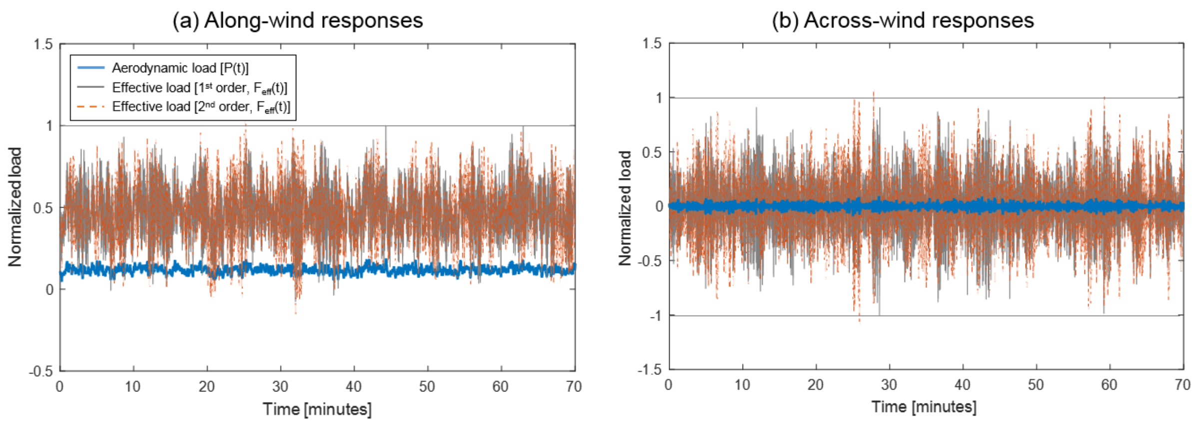

Figure 6. Aerodynamic load and its dynamic internal responses

The second-order effects on the overturning moment in the along-wind and the across-wind directions were investigated. The effective overturning moment and the wind-induced overturning moments were calculated by summing up moments at the base induced by the effective force and by the wind force alone, acting at all floors. Figure 7 shows the spectral densities of the along-wind and across-wind overturning moments at wind speeds U_{ref} = 20 m/s, 60 m/s, and 100 m/s with wind direction θ = 90°. The solid blue (dim gray shown in grayscale) and orange (gray) areas represent the effective overturning moments in the analyses without and with second-order effects, respectively, and the solid gray (light gray) area indicate the overturning moments induced by the wind forces alone. In the case of along-wind overturning moments (left plots in Figure 7), noticeable background responses are significant. The effective overturning moments show resonant responses at the natural frequencies at which the directional wind generates dominant vibration modes while the wind-induced moment does not have a resonant part. Note that the resonance response in the effective moment occurs at a lower frequency in the second-order analysis than that in the first-order analysis. In the case of across-wind overturning moments (right plots in Figure 7), the peak responses of the effective overturning moments occur not only at the natural frequencies, but also at a frequency related to vortex shedding. The effect of vortex shedding on the across-wind loads is clearly seen under all cases. When the reference wind speed is 20 m/s, the peak frequencies of the effective moments (i.e., the natural frequencies) are not close to the frequency of the across-wind moment. As wind speed increases, however, the vortex shedding frequency gets closer to the natural frequency of the building. Resonance then occurs in the response with second-order effects at U_{ref} = 100 m/s (Figure 7c), when the vortex shedding frequency is close to the 2nd and the 3rd natural frequencies, both of which are approximately 0.165 Hz. Note that these two frequencies are almost identical in the second-order analysis (see Table 1). This explains why the across-wind overturning moment in the *y* direction can increase significantly when the 100 m/s wind is acting on the building along the *y* direction.

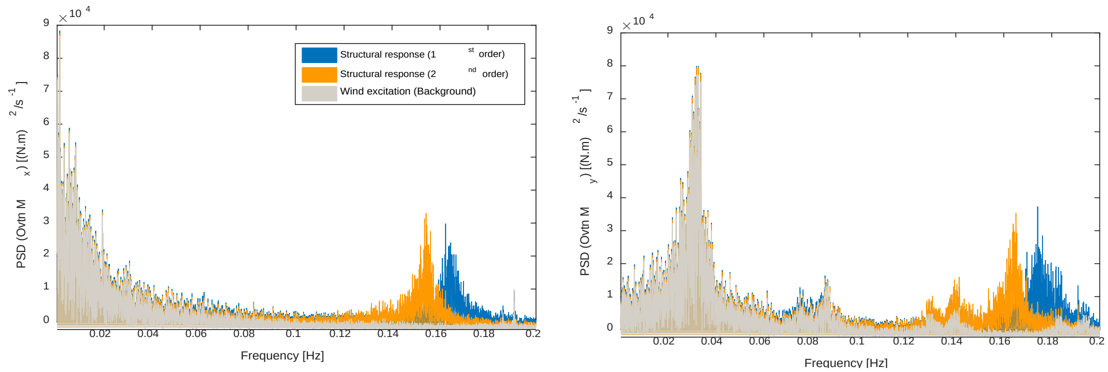

(a) 20 m/s

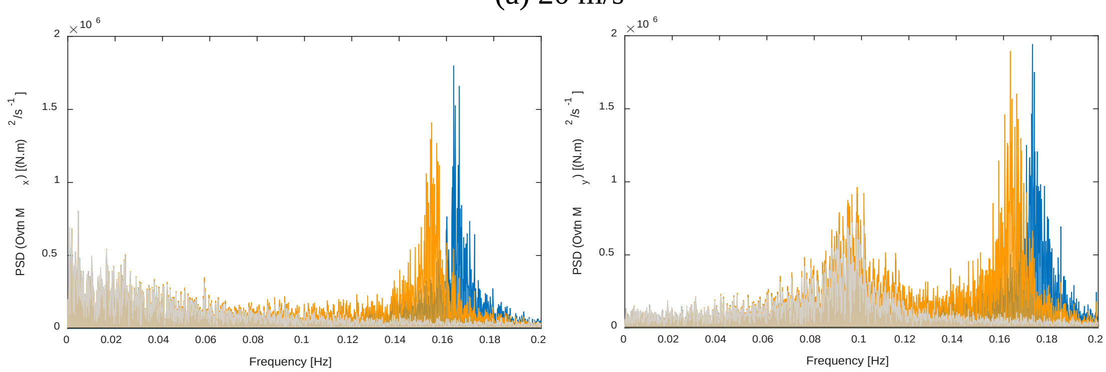

(b) 60 m/s

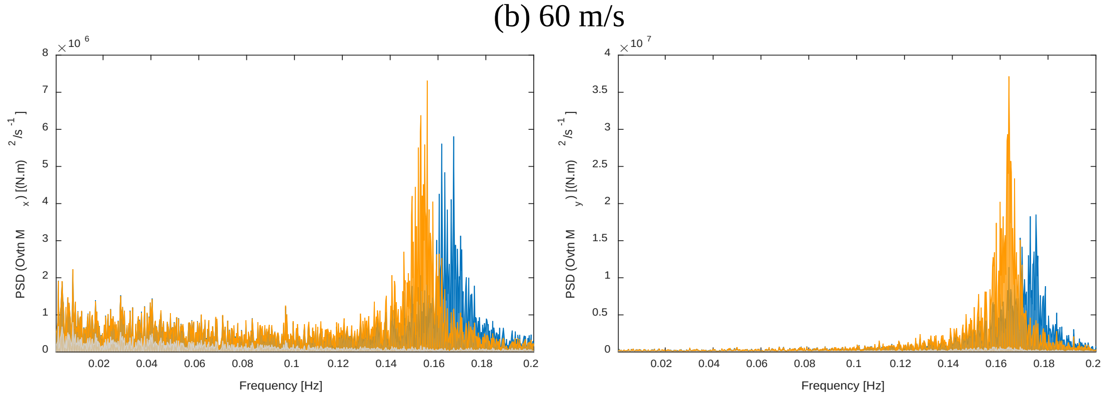

(c) 100 m/s

Figure 7. Frequency distributions of wind excitation and overturning moments with respect to hourly mean winds (left: along-wind resp.; right: across-wind resp.)

Figure 8 and Table 2 show the second-order effects on the overturning moment coefficient. The along- and across-wind peak overturning moments are shown as functions of wind speed *V* and wind direction θ:

$$C_{Mx}(V,\theta) \text{ or } C_{My}(V,\theta) = \frac{M_{ovtn,x}(V,\theta) \text{ or } M_{ovtn,y}(V,\theta)}{\frac{1}{2}\rho V^2 BH^2} \tag{8}$$

where $M_{ovtn,x}$ and $M_{ovtn,y}$ are the overturning moments in x- and y-direction, respectively, ρ is the air density, B is the wide dimension of the building, and H is the height of the building. When the wind direction is 0°, the across-wind moments are larger than the along-wind moments, while both moments at 90° wind direction are nearly equal to a wind speed of 80 m/s. In the case of θ = 90° and U_{ref} = 100 m/s, the ratio of the across-wind moment with second-order effect to its counterpart without it is 1.56. This is due to the resonance induced by vortex shedding when the second-order effects are considered. The case of 90 m/s wind speed is also included in Figure 8.

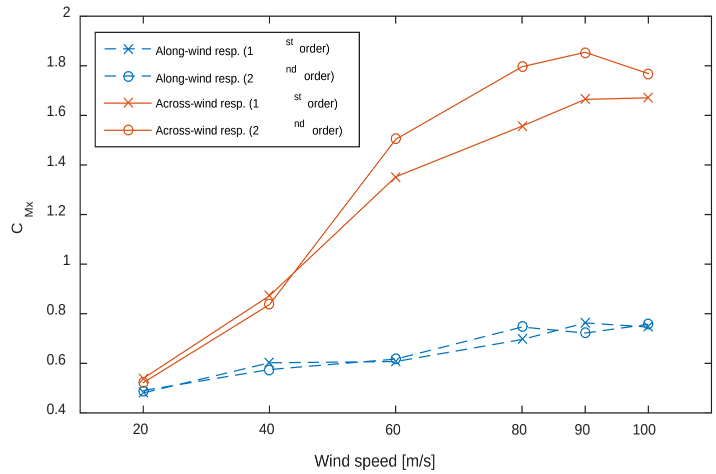

(a) Wind direction of 0°

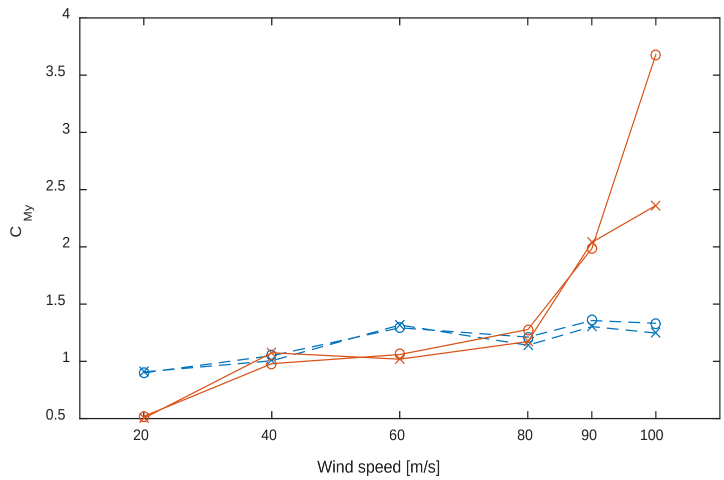

(b) Wind direction of 90°

Figure 8. Peak effective overturning moment coefficients under along- and across-wind responses

Table 2. Second-order effects on the Peak effective overturning moment coefficients under along- and across-wind responses

θ	Along-wind M_{ovtn} [N.m] under LC1						Across-wind M_{ovtn} [N.m] under LC1					
	20 m/s		60 m/s		100 m/s		20 m/s		60 m/s		100 m/s	
0°	1.02 [a]	0.49 [b] 0.48 [c]	1.02	0.62 0.61	1.01	0.76 0.75	0.97	0.52 0.54	1.11	1.50 1.35	1.06	1.77 1.67
90°	0.99	0.90 0.91	0.98	1.29 1.32	1.07	1.33 1.25	1.03	0.52 0.50	1.04	1.06 1.02	1.56	3.68 2.36

[a]Ratio of peak effective M_{ovtn} coefficients with 2nd order effect to the counterpart with 1st order effect (b/c).
[b]Peak effective M_{ovtn} coefficient with 2nd order effect.
[c]Peak effective M_{ovtn} coefficient with 1st order effect.

The second-order effects are investigated for the shear force coefficients (C_{Fx} and C_{Fy}) and the overturning moment coefficients (C_{Mx} and C_{My}) in the *x*- and *y*-directions, respectively, and torsional moment coefficient (C_T) at the base of the structure. The shear force and torsional moment coefficients are defined as:

$$C_{Fx}(V,\theta) \text{ or } C_{Fy}(V,\theta) = \frac{F_x(V,\theta) \text{ or } F_y(V,\theta)}{\frac{1}{2}\rho V^2 BH} \text{ and } C_T(V,\theta) = \frac{T_z(V,\theta)}{\frac{1}{2}\rho V^2 BH^2} \tag{9}$$

where F_x and F_y are the base shear forces in the *x*- and *y*-direction, respectively, and T_z is the base torsional moment in the *z*-direction. Figures 9 and 10 show those shear force and torsional moment coefficients at the base as a function of wind direction in the wind speed of U_{ref} = 60 m/s. The symbols represent the mean values of force and moment coefficients and the bars crossing these symbols indicate a range from their minimum to maximum peak values. Note that the directions for the along-wind and for the across-wind responses are 0° and 90° for C_{Fx} and C_{My}, and 90° and 0° for C_{Fy} and C_{Mx}, respectively. The results show no second-order effects on the mean values, however differences in peak values are significant and are of interest from a structural design viewpoint. The across-wind shear forces and overturning moment fluctuations are stronger than their along-wind counterparts. This is due to the vortex-induced wind forces in the across-wind direction. The fluctuations with second-order effects are larger in most cases, especially when the wind directions are aligned with the principal axes of the building (i.e., θ = 0° and 90°). In addition, the torsional moments have the largest negative and positive mean values for θ = 10° and 70°, respectively. This was also observed by Matsumoto et al. (1998), and was attributed to a separation point shift. Wind-induced torsional responses will be significant when a building has the mass center at each floor offset from its elastic center.

Table 3 summarizes the effects of secondary action on non-directional peak base shears and overturning moments based on the reference wind speeds under LC1. The peak values in the table are defined as the non-directional peak values (i.e., the largest of all directional peak values calculated from all wind directions). From a practical design viewpoint, it is reasonable to use the non-directional peak values for assessing the second-order effects. As shown in the table, the second-order effects are generally on the order of 10 % to 15 % of the first-order effects at wind speeds up to U_{ref} = 80 m/s. In the case of U_{ref} = 100 m/s, the peak overturning moment in y-direction ($M_{ovtn,y}$) is increased by approximately 50 % by the second-order effects when the wind direction is θ = 90°. This is due to the vortex-induced resonance, as seen in Figure 7(c).

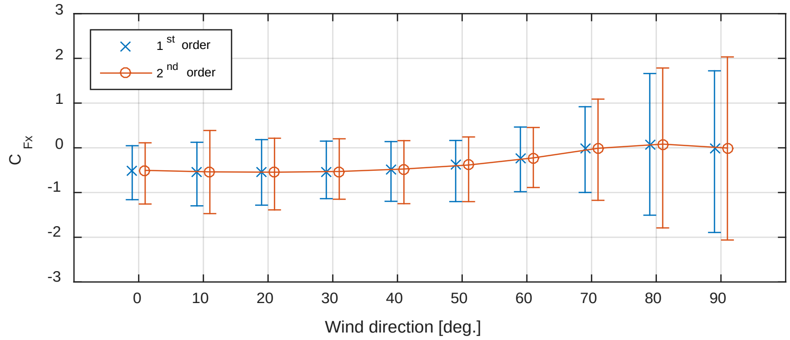

(a) C_{Fx}

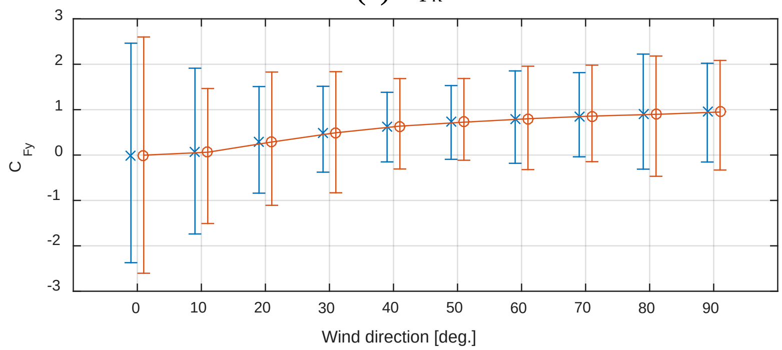

(b) C_{Fy}

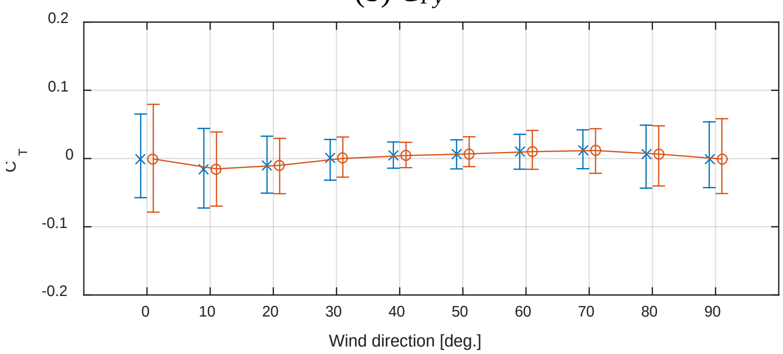

(c) C_T

Figure 9. Force coefficients as a function of wind direction (U_{ref} = 60 m/s)

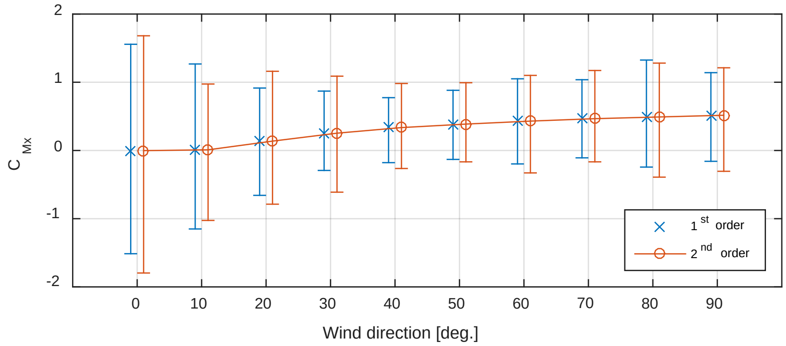

(a) C_{Mx}

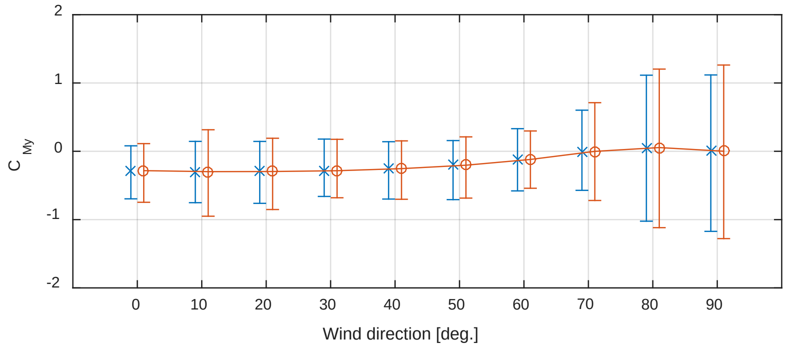

(b) C_{My}

Figure 10. Moment coefficients as a function of wind direction (U_{ref} = 60 m/s)

Table 3. Second-order effects on the peak base shears and overturning moments

Forces and moments	Reference wind speeds (U_{ref}) under LC1									
	20 m/s		40 m/s		60 m/s		80 m/s		100 m/s	
F_x	0.98[a]	1.94E+06[b] 1.98E+06[c]	0.91	1.32E+07 1.45E+07	1.08	3.16E+07 2.91E+07	1.09	6.76E+07 6.20E+07	1.52	2.86E+08 1.88E+08
F_y	1.02	3.55E+06 3.48E+06	0.92	1.55E+07 1.69E+07	1.03	4.12E+07 4.02E+07	1.06	8.54E+07 8.08E+07	1.04	1.35E+08 1.29E+08
T_z	0.92	1.56E+07 1.70E+07	1.11	8.80E+07 7.90E+07	0.99	2.23E+08 2.25E+08	1.10	4.76E+08 4.35E+08	1.40	1.23E+09 8.74E+08
$M_{ovtn,x}$	1.00	3.43E+08 3.43E+08	0.89	1.57E+09 1.77E+09	1.11	5.07E+09 4.56E+09	1.15	1.08E+10 9.33E+09	1.06	1.66E+10 1.56E+10
$M_{ovtn,y}$	1.03	1.95E+08 1.89E+08	0.91	1.47E+09 1.61E+09	1.04	3.57E+09 3.44E+09	1.09	7.66E+09 7.03E+09	1.56	3.45E+10 2.21E+10

[a] Ratio of peak non-directional base shear or moment with 2nd order effect to the counterpart with 1st order effect (= b/c).
[b] Peak base shears or moments with 2nd order effect.
[c] Peak base shears or moments with 1st order effect.

3.3. Strength design: Demand-to-Capacity Index (DCI)

Response databases of demand-to-capacity indexes were calculated in the two load combination cases (LC1 and LC2 in Eq. 5) for 21 selected structural members: 9 columns, 9 beams, and 3 diagonal bracings (see Figure 3d) consisting of 1) three core columns (CO1, CO3, CO5), three corner columns (CC1, CC3, CC5), and three external columns (CE1, CE3, CE5), on 1st, 21st, and 41st stories, 2) three external beams (BE1, BE3, BE5), three internal beams (BI1, BI3, BI5), and three core beams (BO1, BO3, BO5), on 10th, 30th, and 50th floors, and three core bracings (XO1, XO3, XO5) on 1st, 21st, and 41st stories. Their DCIs for interaction of axial forces and bending moments (B_{ij}^{PM}) and for shear forces (B_{ij}^{V}) were calculated with wind directions (θ = 0°, 10°, ..., 350°) and wind speeds (U_{ref} = 60 m/s, 80 m/s, and 100 m/s). Figure 11 shows an example of the response databases of B_{ij}^{PM} and B_{ij}^{V} for the corner column at the 1st story (CC1) under LC1. The DCI values in the response databases are the peak values of a time-series of DCIs calculated in Eqs. A1 to A4.

Tables 4 and 5 summarize the second-order effects on non-directional peak DCIs for the selected members in the two load combination cases, and Figure 12 and 13 illustrate their second-order effect ratios. Overall, the maximum B_{ij}^{PM} values are larger in LC1 than in LC2, but the maximum B_{ij}^{V} values in LC1 are as high as those in LC2. In Table 4, most of the peak B_{ij}^{PM} values are over unity, and they are even higher than 9 for a certain wind speed. This is due not only to use of consistent structural members of the building under various wind speeds, but also to the limitations of the elastic analysis performed in this study.

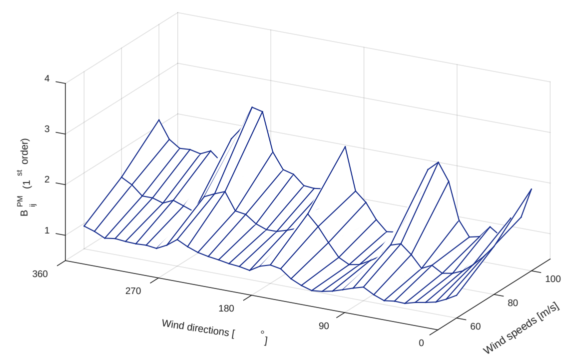

(a) B_{ij}^{PM} from 1st order analysis

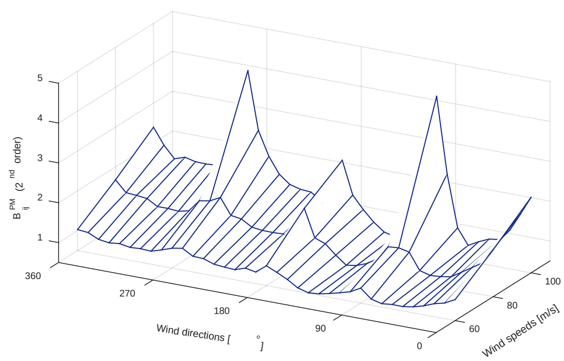

(b) B_{ij}^{PM} from 2nd order analysis

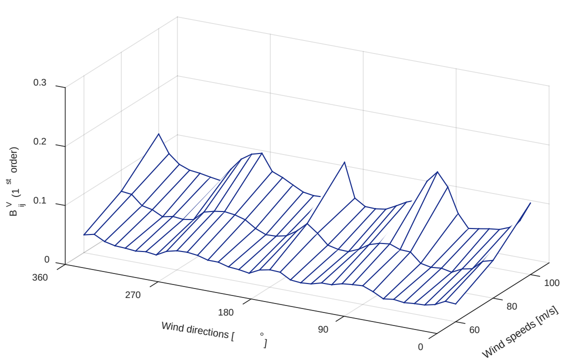

(c) B_{ij}^{V} from 1st order analysis

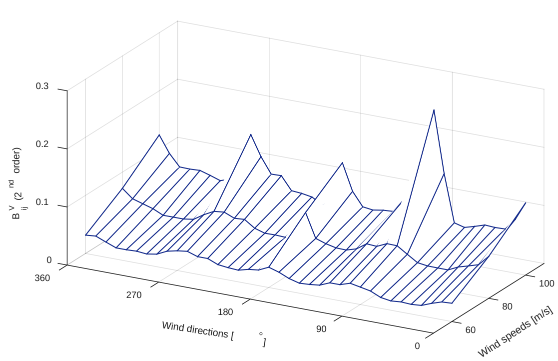

(d) B_{ij}^{V} from 2nd order analysis

Figure 11. Response databases: B_{ij}^{PM} and B_{ij}^{V} (member label = CC1)

Table 4. Peak DCI (B_{ij}^{PM}) for two load combinations and second-order effects

Member	Label	Story (floor)	Reference wind speed (U_{ref})					
			60 m/s		80 m/s		100 m/s	
			Ratio [a]	LC1 (LC2)	Ratio	LC1 (LC2)	Ratio	LC1 (LC2)
Corner column (CC)	CC1	1st	1.02	1.04 (0.85) [b] 1.02 (0.83) [c]	1.19	1.84 (1.48) 1.54 (1.35)	1.66	4.49 (4.29) 2.71 (2.51)
	CC3	21st	1.04	0.99 (0.81) 0.95 (0.77)	1.14	1.66 (1.32) 1.45 (1.27)	1.61	4.18 (4.00) 2.60 (2.41)
	CC5	41st	1.04	0.92 (0.74) 0.89 (0.71)	1.14	1.54 (1.22) 1.35 (1.17)	1.65	3.86 (3.65) 2.34 (2.16)
Exterior column (CE)	CE1	1st	1.04	0.99 (0.76) 0.96 (0.72)	1.15	1.54 (1.30) 1.33 (1.10)	1.65	4.21 (3.97) 2.55 (2.31)
	CE3	21st	1.03	0.91 (0.70) 0.88 (0.67)	1.17	1.42 (1.21) 1.22 (1.01)	1.66	4.12 (3.91) 2.49 (2.28)
	CE5	41st	1.03	0.92 (0.70) 0.90 (0.67)	1.14	1.41 (1.19) 1.23 (1.01)	1.62	4.06 (3.84) 2.51 (2.29)
Core column (CO)	CO1	1st	1.04	2.05 (1.83) 1.98 (1.75)	1.16	3.77 (3.54) 3.26 (3.03)	1.60	10.17(9.94) 6.34 (6.11)
	CO3	21st	1.07	1.45 (1.24) 1.36 (1.15)	1.15	2.53 (2.32) 2.20 (2.00)	1.62	6.80 (6.59) 4.18 (3.98)
	CO5	41st	1.05	1.23 (0.98) 1.17 (0.91)	1.16	2.06 (1.81) 1.77 (1.51)	1.62	4.83 (4.57) 2.99 (2.73)
Internal beam (BI)	BI1	10th	1.12	1.09 (0.81) 0.98 (0.69)	1.25	1.65 (1.36) 1.31 (1.03)	1.30	2.30 (2.07) 1.77 (1.48)
	BI3	30th	1.11	1.27 (0.93) 1.14 (0.80)	1.23	1.83 (1.49) 1.49 (1.15)	1.26	2.52 (2.34) 2.01 (1.67)
	BI5	50th	1.08	1.23 (0.86) 1.14 (0.77)	1.09	1.62 (1.25) 1.49 (1.11)	1.10	2.07 (1.93) 1.89 (1.51)
External beam (BE)	BE1	10th	1.21	0.80 (0.67) 0.66 (0.53)	1.41	1.46 (1.33) 1.04 (0.91)	1.30	2.26 (2.13) 1.74 (1.61)
	BE3	30th	1.25	0.87 (0.74) 0.70 (0.56)	1.39	1.57 (1.44) 1.13 (1.00)	1.18	2.17 (2.04) 1.84 (1.71)
	BE5	50th	1.20	0.74 (0.60) 0.62 (0.48)	1.24	1.23 (1.10) 0.99 (0.86)	1.14	1.68 (1.55) 1.48 (1.34)
Core beam (BO)	BO1	10th	1.09	0.81 (0.52) 0.74 (0.49)	1.15	1.06 (0.80) 0.92 (0.67)	1.62	2.47 (2.21) 1.52 (1.27)
	BO3	30th	1.07	0.76 (0.48) 0.71 (0.45)	1.11	0.95 (0.69) 0.85 (0.60)	1.58	2.09 (1.84) 1.33 (1.07)
	BO5	50th	1.02	0.68 (0.41) 0.67 (0.41)	1.05	0.79 (0.54) 0.76 (0.50)	1.39	1.42 (1.16) 1.02 (0.76)
Core bracing (XO)	XO1	1st	1.05	0.52 (0.47) 0.49 (0.46)	1.08	0.93 (0.89) 0.87 (0.84)	1.30	2.16 (2.13) 1.67 (1.62)
	XO2	21st	1.13	0.64 (0.61) 0.57 (0.52)	1.23	1.34 (1.31) 1.10 (1.05)	1.22	2.05 (2.02) 1.68 (1.64)
	XO3	41st	1.16	0.96 (0.92) 0.83 (0.77)	1.31	2.01 (1.96) 1.54 (1.47)	1.14	2.92 (2.88) 2.55 (2.49)

[a] The larger value of ratios of peak non-directional DCIs with 2nd order effect to the counterpart with 1st order effect, in respective LC1 and LC2.
[b] Peak DCI with 2nd order effect.
[c] Peak DCI with 1st order effect.

Table 5. Peak DCI (B_{ij}^{V}) for two load combinations and second-order effects

Member	Label	Story (floor)	Reference wind speed (U_{ref})					
			60 m/s		80 m/s		100 m/s	
			Ratio [a]	LC1 (LC2)	Ratio	LC1 (LC2)	Ratio	LC1 (LC2)
Corner column (CC)	CC1	1st	1.07	0.037 (0.036) [b] 0.034 (0.034) [c]	1.30	0.089 (0.088) 0.068 (0.067)	1.77	0.258 (0.254) 0.145 (0.146)
	CC3	21st	1.48	0.067 (0.065) 0.045 (0.043)	1.67	0.148 (0.145) 0.089 (0.086)	1.97	0.476 (0.477) 0.241 (0.239)
	CC5	41st	1.46	0.076 (0.070) 0.052 (0.046)	1.48	0.153 (0.147) 0.103 (0.098)	1.96	0.458 (0.461) 0.234 (0.231)
Exterior column (CE)	CE1	1st	1.11	0.038 (0.037) 0.034 (0.034)	1.32	0.090 (0.089) 0.068 (0.068)	1.50	0.199 (0.186) 0.133 (0.133)
	CE3	21st	1.18	0.054 (0.051) 0.046 (0.042)	1.42	0.121 (0.121) 0.085 (0.082)	1.79	0.386 (0.448) 0.252 (0.249)
	CE5	41st	1.11	0.068 (0.059) 0.061 (0.052)	1.11	0.124 (0.118) 0.112 (0.103)	1.77	0.443 (0.504) 0.290 (0.281)
Core column (CO)	CO1	1st	1.07	0.093 (0.092) 0.087 (0.087)	1.18	0.207 (0.207) 0.175 (0.175)	1.70	0.681 (0.681) 0.400 (0.400)
	CO3	21st	1.38	0.160 (0.160) 0.116 (0.116)	1.39	0.342 (0.342) 0.246 (0.247)	1.93	1.273 (1.272) 0.660 (0.660)
	CO5	41st	1.35	0.093 (0.092) 0.069 (0.068)	1.37	0.198 (0.199) 0.146 (0.145)	1.89	0.717 (0.714) 0.379 (0.377)
Internal beam (BI)	BI1	10th	1.05	0.409 (0.266) 0.388 (0.245)	1.13	0.507 (0.364) 0.448 (0.305)	1.18	0.623 (0.490) 0.528 (0.386)
	BI3	30th	1.05	0.439 (0.287) 0.417 (0.265)	1.13	0.540 (0.388) 0.479 (0.327)	1.16	0.663 (0.539) 0.572 (0.420)
	BI5	50th	1.04	0.434 (0.275) 0.418 (0.259)	1.05	0.503 (0.344) 0.479 (0.321)	1.06	0.582 (0.466) 0.551 (0.392)
External beam (BE)	BE1	10th	1.11	0.251 (0.181) 0.226 (0.157)	1.26	0.370 (0.300) 0.295 (0.225)	1.22	0.511 (0.440) 0.419 (0.349)
	BE3	30th	1.13	0.264 (0.194) 0.233 (0.163)	1.25	0.388 (0.318) 0.310 (0.240)	1.13	0.496 (0.426) 0.437 (0.368)
	BE5	50th	1.10	0.240 (0.170) 0.219 (0.149)	1.15	0.328 (0.258) 0.286 (0.216)	1.10	0.408 (0.338) 0.372 (0.302)
Core beam (BO)	BO1	10th	1.03	0.358 (0.220) 0.346 (0.208)	1.06	0.403 (0.265) 0.378 (0.240)	1.35	0.653 (0.515) 0.485 (0.347)
	BO3	30th	1.02	0.349 (0.211) 0.340 (0.202)	1.04	0.382 (0.244) 0.366 (0.228)	1.30	0.586 (0.449) 0.450 (0.312)
	BO5	50th	1.01	0.335 (0.197) 0.332 (0.195)	1.02	0.355 (0.218) 0.349 (0.211)	1.18	0.467 (0.329) 0.396 (0.258)
Core bracing (XO)	XO1	1st	1.05	0.032 (0.028) 0.031 (0.026)	1.11	0.056 (0.052) 0.050 (0.046)	1.80	0.175 (0.172) 0.097 (0.093)
	XO2	21st	1.05	0.016 (0.012) 0.016 (0.012)	1.13	0.028 (0.024) 0.024 (0.020)	1.84	0.093 (0.089) 0.050 (0.046)
	XO3	41st	1.10	0.017 (0.012) 0.016 (0.011)	1.11	0.024 (0.019) 0.021 (0.016)	1.55	0.052 (0.047) 0.033 (0.028)

[a] The larger value of ratios of peak non-directional DCIs with 2nd order effect to the counterpart with 1st order effect, in respective LC1 and LC2.
[b] Peak DCI with 2nd order effect.
[c] Peak DCI with 1st order effect.

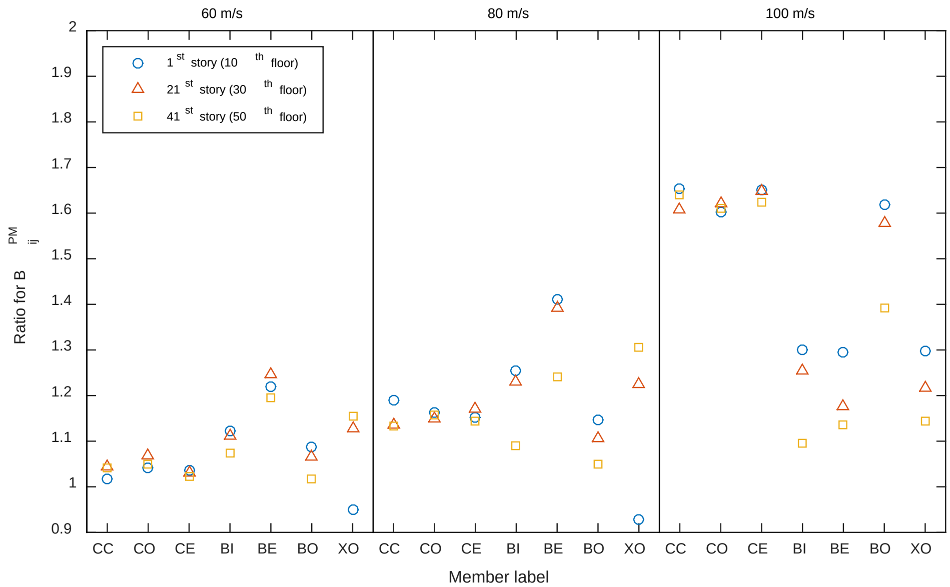

Figure 12. 2nd order effect ratios for $B_{ij}{}^{PM}$ depending on member types and wind speeds

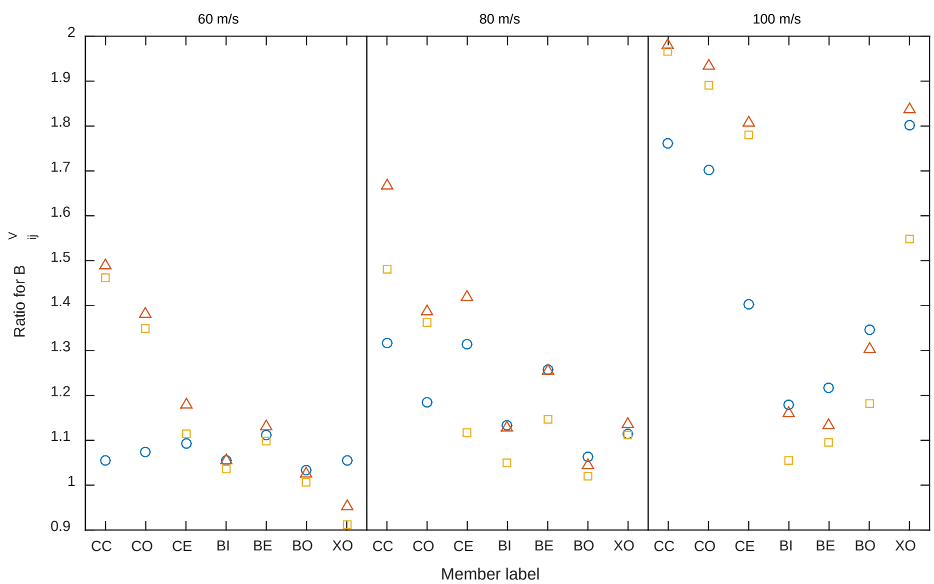

Figure 13. 2nd order effect ratios for $B_{ij}{}^{V}$ depending on member types and wind speeds

As shown in Tables 4-5 and Figures 12-13, the second-order effects on axial loads and moments (i.e., $B_{ij}{}^{PM}$) of all columns are less than 7 % for U_{ref} = 60 m/s. However, they increase by up to 19 % for U_{ref} = 80 m/s and by approximately 66 % for U_{ref} = 100 m/s. In the case of $B_{ij}{}^{PM}$ for beams, the second-order effects increase by up to 30 % for external and internal beams (BE and BI) for all reference wind speeds. However, the second-order effects on the core beam (BO) is much larger, up to 62 %, than for the other selected beams. For U_{ref} = 100 m/s with θ = 90°, the DCI values of all columns, core beams, and core bracings increase by 14 % to 66 % because vortex-induced across-wind fluctuations lead to increased axial forces and bending moments in their members.

The demand-to-capacity indexes for shears, B_{ij}^{V}, are less than 0.7 in all cases, considerably lower than B_{ij}^{PM}. The second-order effects on all columns increase with wind speeds up to 48 %, 67 %, and 97 % for U_{ref} = 60 m/s, 80 m/s, and 100 m/s, respectively. In the case of beams, the second-order effects are up to 35 % larger for all wind speeds. Note that the B_{ij}^{V} values of most members are considerably smaller than the B_{ij}^{PM}, which means B_{ij}^{V} is not the critical factor in the structural design of the building considered in this study.

3.4. Serviceability design: Inter-story drift and acceleration

Response databases for inter-story drifts and accelerations were calculated in the load combination case of LC3 (Eq. 6) along a column line of interest for serviceability design (see Figure 3d). The reference wind speeds were taken as 20 m/s, 40 m/s, and 60 m/s for the analysis for serviceability. Details on expressions for the inter-story drift ratio and the acceleration for the building are provided in Appendix 2. Figure 14 shows the inter-story drift ratios in both *x*- and *y*-direction corresponding to the across- and the along-wind response, respectively, along the column line when the reference wind speed is U_{ref} = 40 m/s and the wind direction is θ = 90°. As shown in the figure, the second-order effect increases the inter-story drifts by up to 30 % and 17 % in the along- and across-wind response, respectively. Note that the inter-story drift ratios are less than 0.001 on 20th, 21st, 40th, and 41st stories where the outrigger and belt truss systems are located. Figure 15 plots the peak inter-story drift ratios from all stories as a function of wind direction and shows that the second-order effect increases inter-story drifts in most wind directions. Since the selected column line is located at the lower right-hand corner of the building plane (see Fig. 3d), the peak inter-story drifts for *x*- and *y*-direction is symmetry with the wind directions of 90° and 270° in Fig. 15a and with 180° in Fig. 15b, respectively. Note that the *x*-direction inter-story drift at wind direction of 10° is larger than that of 0°, which can be explained by the reattachment of wind flows on the rectangular section of the building as previously mentioned in Section 3.2. The behavior is also observed in the *y*-direction inter-story drift for wind directions between 80° and 90°.

Figures 16 and 17 show the resultant accelerations for the column line at the wind direction of 90° and the top-floor accelerations with respect to wind directions, respectively, when the reference wind speed is 40 m/s. The unit of acceleration used in the figures is milli-g, where g is the gravitational acceleration (9.81 m/s^2). As shown in the Figure 16, the second-order effect can be noticeable only above approximately the top half floors and increases top-floor accelerations by 2 %.

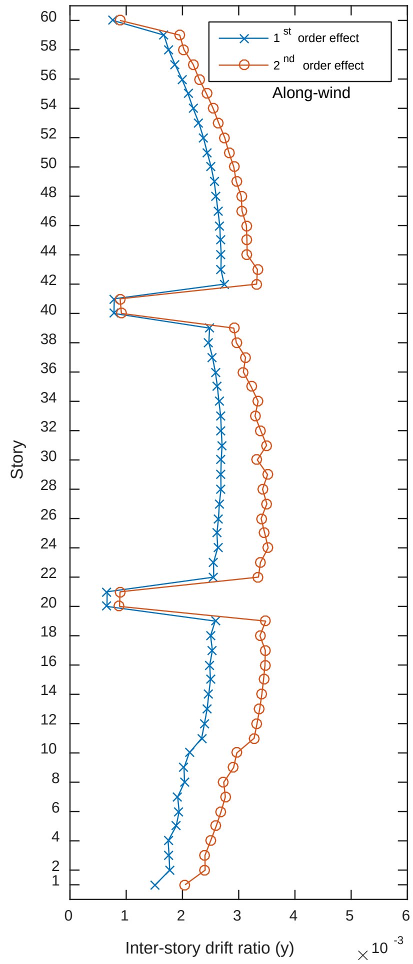

(a) Along-wind response

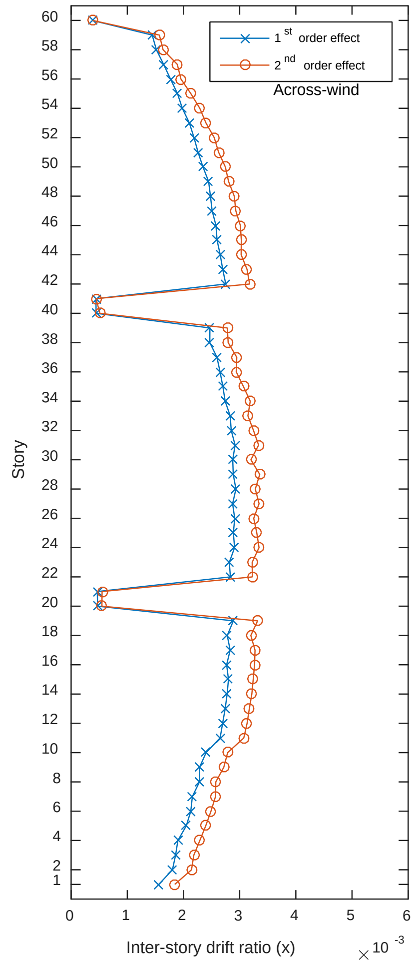

(b) Across-wind response

Figure 14. Inter-story drifts along the column line (U_{ref} = 40 m/s, θ = 90°)

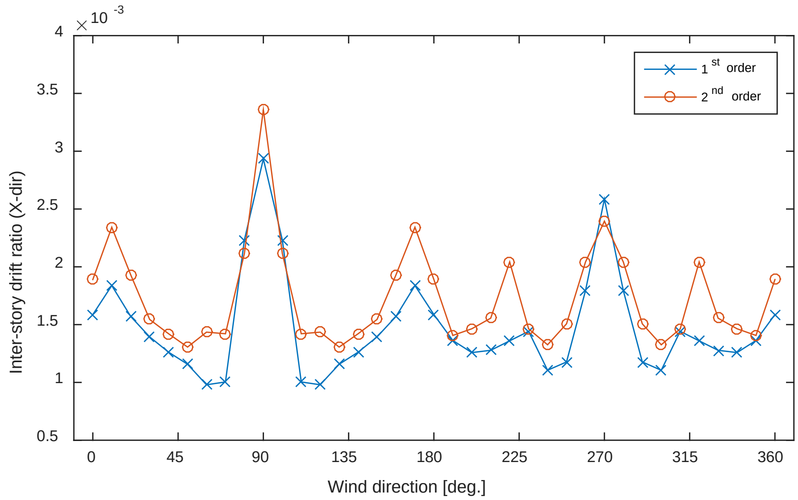

(a) Along the *x*-direction

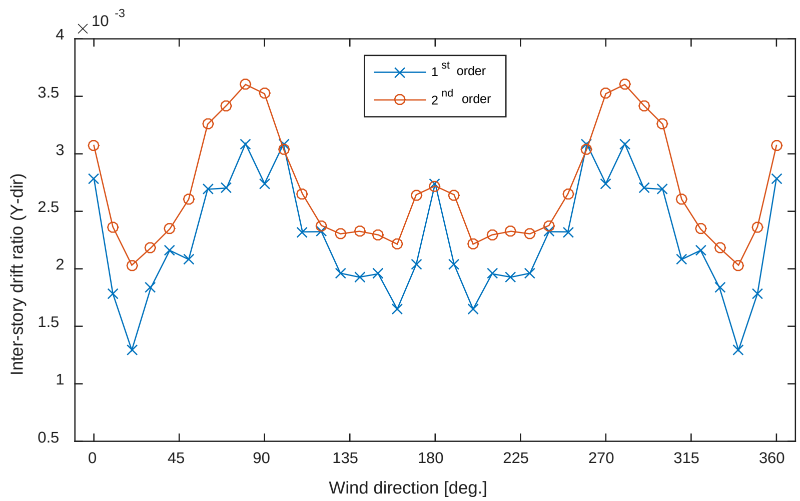

(b) Along the *y*-direction

Figure 15. Peak inter-story drifts with respect to wind directions (U_{ref} = 40 m/s)

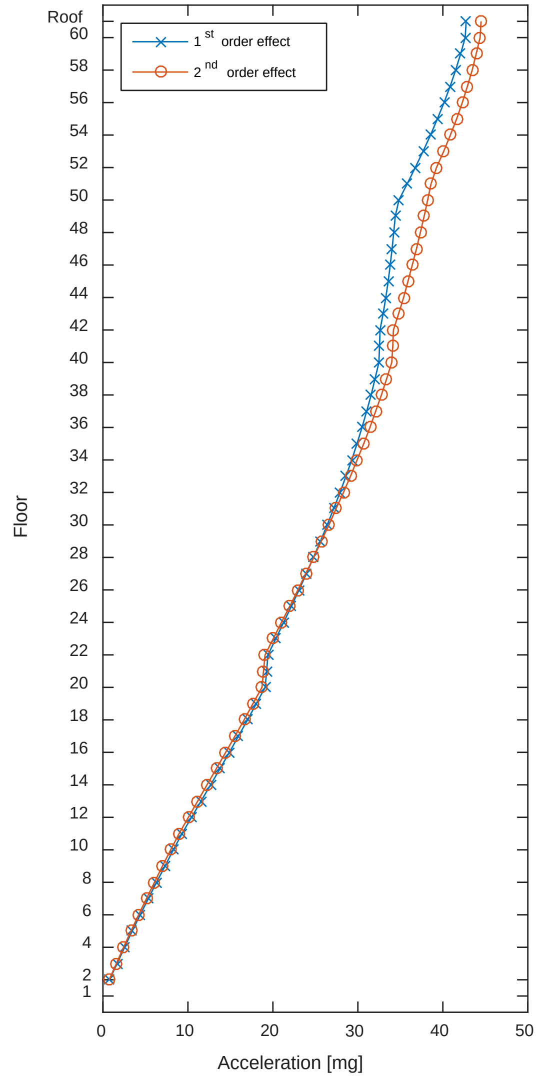

Figure 16. Resultant accelerations for the column line (U_{ref} = 40 m/s, θ = 90°)

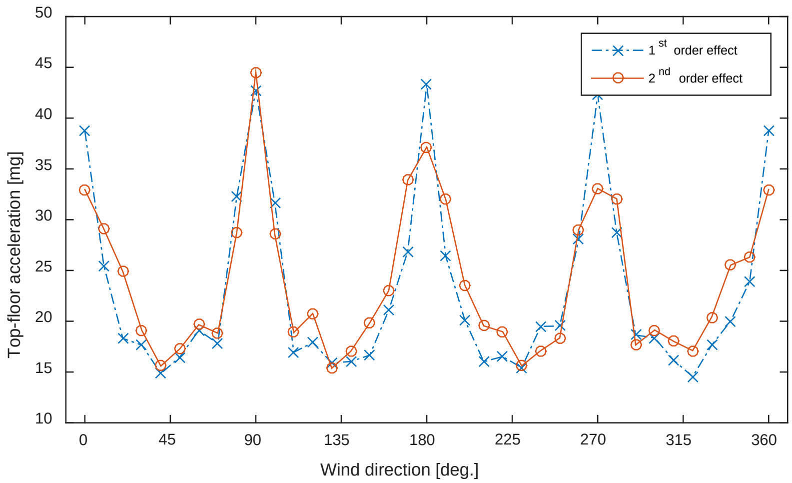

Figure 17. Peak top-floor accelerations with respect to wind directions (U_{ref} = 40 m/s)

Table 6 summarizes the peak inter-story drift ratios and resultant accelerations of the selected column line (Figure 3d) as a function of reference wind speeds, and their second-order effects. The peak values in the table are defined in a manner similar to the peak base shears and overturning moments (see Table 3), as the largest of all directional peak inter-story drift ratios and acceleration values calculated from all wind directions. Based on the results in this case study, the second-order effects increase the inter-story drift ratios by 14 % to 40 % and the resultant accelerations by 2 % to 20 %, respectively. Note that such second-order effects are almost constant at U_{ref} = 20 m/s and 40 m/s, but that they are substantially increased at the highest wind speeds (U_{ref} = 60 m/s).

Table 6. Second-order effects on the peak inter-story drift ratios and top-floor accelerations

Serviceability factors	Reference wind speed (U_{ref}) under LC3					
	20 m/s		40 m/s		60 m/s	
In-dr. ratio in x	1.21 [a]	0.00046 [b]	1.14	0.00336	1.25	0.00748
		0.00038 [c]		0.00293		0.00599
In-dr. ratio in y	1.17	0.00077	1.17	0.00360	1.40	0.01256
		0.00066		0.00309		0.00898
Resultant acc.[d]	1.06	5.37	1.02	44.50	1.20	162.22
		5.06		43.53		134.87

[a] Ratio of peak serviceability factors with 2nd order effect to the counterpart with 1st order effect.
[b] Peak serviceability factors with 2nd order effects.
[c] Peak serviceability factors with 1st order effects.
[d] Unit: milli-g

4. Conclusions

This work presents an investigation into second-order effects on the wind-induced structural dynamic behavior of high-rise steel structure, as considered within a Database-Assisted Design (DAD) context. A geometric stiffness method that accounts for second-order effects and allows the dynamic analysis to be performed without iterations is shown to be applicable in conjunction with DAD and was used in a study of the response of a 60-story building, known as the CAARC building. Datasets of the aerodynamic pressure on the CAARC building for suburban exposure were used to calculate overturning moments and shear forces at the base, as well as members' demand-to-capacity indexes (DCIs), inter-story drift ratios, and resultant accelerations. Under the assumption of linear elastic structural behavior, dynamic analyses of the building were performed for serviceability and strength. The structural behavior was analyzed using global effects (overturning moments, base shear forces, and torsion), as well as local effects: i) for strength design, demand-to-capacity indexes (DCIs) of structural members, ii) for serviceability design, inter-story drift ratios, and resultant accelerations along a column line. Those values were obtained both by considering and disregarding wind directional effects. Of five reference wind speeds at the rooftop of the building (U_{ref} = 20 m/s, 40 m/s, 60 m/s, 80 m/s, and 100 m/s), the first three were used for serviceability analysis, and the last three for strength analysis. The following conclusions can be drawn from this study:

(1) The second-order effects decrease natural frequencies of vibration of the building by up to 12 %. As a result, the 2nd and the 3rd natural frequencies become close to less than 1 %. The first six modes in the modal superposition analysis were shown to be sufficient for accurately assessing the dynamic responses, both when considering and when disregarding second-order effects.

(2) When the wind approaches the building in the principal directions of the building, the second-order effects increase the along-wind peak effective overturning moments by up to 7 % in all wind speeds. However, the across-wind counterparts are increased by up to 11 % in wind speeds of 20 m/s and 60 m/s, and by 56 % in the 100 m/s wind speed. The latter case is significantly influenced by the vortex-induced resonance phenomenon when the vortex shedding frequency is close to the 2nd and the 3rd natural frequencies of the building.

(3) For non-directional second-order effects, the peak base shears are increased by up to 9 %, the torsional moments by up to 10 %, and the overturning moments by up to 15 %, in the non-resonant cases. However, they are increased by 40 % to 56 % in the resonant case of the 100 m/s wind speed and the 90° direction.

(4) For secondary effects on strength of structural members, the DCIs for axial force and bending moments (B_{ij}^{PM}) are increased by up to 19 % for columns, 41 % for beams, and 31 % for diagonal bracings, and those for shear forces (B_{ij}^{V}) by up to 67 % for columns, 26 % for beams, and 13 % for diagonal bracings in the case of U_{ref} = 80 m/s. For U_{ref} = 100 m/s, for which across-wind resonance occurs, the increments due to the second-order effects are 66 %, 62 %, 30 %, 97 %, 35 %, and 84 % respectively. Note that the B_{ij}^{V} values of most members are considerably smaller than the B_{ij}^{PM}, which means B_{ij}^{V} is not the critical factor in the structural design of the building considered in this study.

5) The second-order effects increase the inter-story drift ratios and the resultant accelerations by up to 40 % and 20 %, respectively, in the 60 m/s wind speed. The inter-

story drift ratios show the secondary effects along all stories except ones where the outrigger and belt truss systems are located. However, the secondary effects on the resultant acceleration are shown above approximately the top half floors.

While much research was performed on secondary effects on high-rise building subjected to earthquake loads, this work is, to the authors' knowledge, the first study to focus on the systematic analysis of second-order effects on high-rise buildings subjected to wind loads. The estimates presented in this study were performed to the CAARC building model. However, they show that second-order effects on structural responses of high-rise buildings to wind loads should be analyzed at the design stage. Future research is recommended on estimates of second-order effects that take into account material nonlinearities as well as beam-column joint models in various types of main wind force resisting systems.

References

Al-Mashary, F. and Chen, W. F. (1990). "Elastic second-order analysis for frame design." *Journal of Constructional Steel Research*, 15, 303-322.

ANSI/AISC (2010a). *Specifications for Structural Steel Buildings*, AISC 360-10, American Institute of Steel Construction, Chicago, Illinois.

ANSI/AISC (2010b). *Steel construction manual*, 14th ed., American Institute of Steel Construction.

ASCE (1988). "Wind Drift Design of Steel-framed Buildings: State-of-the-art Report, ASCE Task Committee on Drift Control of Steel Building Structures of the Committee on Design of Steel Building Structures." *Journal of Structural Engineering*, 114(9), 2085-2108.

ASCE (2010). *Minimum design loads for buildings and other structures*, ASCE 7-10, American Society of Civil Engineers, Reston, VA.

ASCE (2016). *Minimum design loads for buildings and other structures*, ASCE 7-16 (due for publication in Fall 2016), American Society of Civil Engineers, Reston, VA.

Baji, H., Ronagh, H. R., Shayanfar, M. A., and Barkhordari, M. A. (2012). "Effect of Second Order Analysis on the Drift Reliability of Steel Buildings." *Advances in Structural Engineering*, 15(11), 1989-1999.

Berding, D. C. (2006). *Wind drift design of steel framed buildings: An analytical study and a survey of the practice*, Virginia Polytechnic Institute and State University, Blacksburg, VA.

Bernal, D. (1998). "Instability of buildings during seismic response." *Engineering Structures*, 20(4–6), 496-502.

Chen, W. F. and Lui, E. M. (1987). *Structural Stability: Theory Implementation*, 1st ed., Prentice Hall.

CSI (2015). Integrated Finite Element Analysis and Design of Structures, v.17.

Goto, Y. and Chen, W. F. (1987). "Second-order elastic analysis for frame design." *Journal of Structural Engineering*, 113(7), 1501-1519.

Gupta, A. and Krawinkler, H. (2000). "Dynamic P-Delta Effects for Flexible Inelastic Steel Structures." *Journal of Structural Engineering*, 126(1), 145-154.

Humar, J., Mahgoub, M., and Ghorbanie-Asl, M. (2006). "Effect of second-order forces on seismic response." *Canadian Journal of Civil Engineering*, 33(6), 692-706.

LeMessurier, W. J. (1976). "A practical method of second order analysis, Part 1 - Pin-jointed frames." *Engineering journal, AISC*, 13(4), 89-96.

LeMessurier, W. J. (1977). "A practical method of second order analysis, Part 2 - Rigid Frames." *Engineering journal, AISC*, 14(2), 49-67.

MacRae, G. A. (1993). "P-delta design in seismic regions." *La Jolla, Calif.: Dept. of Applied Mechanics & Engineering Sciences, University of California, San Diego.*

Matsumoto, M., Ishizakia, H., Matsuokab, C., Daitoc, Y., Ichikawaa, Y., and Shimaharaa, A. (1998). "Aerodynamic effects of the angle of attack on a rectangular prism." *Journal of Wind Engineering and Industrial Aerodynamics*, 77-78(1), 531-542.

Melbourne, W. H. (1980). "Comparison of measurements on the CAARC standard tall building model in simulated model wind flows." *Journal of Wind Engineering and Industrial Aerodynamics*, 6(1), 73-88.

Newmark, N. M. and Rosenblueth, E. (1971). *Fundamentals of Earthquake Engineering*, ed., Prentice Hall, Englewood Cliffs, New Jersey.

Rutenberg, A. (1981). "A direct P-delta analysis using standard plane frame computer programs." *Computers & Structures*, 14(1-2), 97-102.

Simiu, E. (2011). *Design of buildings for wind: A guide for ASCE 7-10 standard users and designers of special structures*, 2nd ed., John Wiley & Sons, Inc., Hoboken, New Jersey.

Simiu, E., Gabbai, R. D., and Fritz, W. P. (2008). "Wind-induced tall building response: A time-domain approach." *Wind and Structures*, 11(6), 427-440.

Tremblay, R., Léger, P., and Tu, J. (2001). "Inelastic seismic response of concrete shear walls considering P-delta effects." *Canadian Journal of Civil Engineering*, 28(4), 640-655.

Venanzi, I. (2005). "Analysis of the torsional response of wind-excited high-rise building." *Ph. D. dissertation, Universita degli Studi di Perugia, Perugia.*

White, D. W. and Hajjar, J. F. (1991). "Application of second-order elastic analysis in LRFD: research to practice." *Engineering Journal*, 28(4), 133-148.

Williamson, E. (2003). "Evaluation of Damage and P-Δ Effects for Systems Under Earthquake Excitation." *Journal of Structural Engineering*, 129(8), 1036-1046.

Wilson, E. L. and Habibullah, A. (1987). "Static and Dynamic Analysis of Multi-Story Buildings, Including P-Delta Effects." *Earthquake Spectra*, 3(2), 289-298.

Wood, B. R., Beaulieu, D., and Adams, P. F. (1976). "Column design by P-delta method." *Journal of the Structural Division*, 102(2), 411-427.

Yeo, D. (2010). "Database-Assisted Design of high-rise reinforced concrete structures for wind: Concepts, software, and application." *NIST Technical Note 1665, National Institute of Standards and Technology, Gaithersburg, MD.*

Yeo, D. (2013). "Multiple Points-In-Time Estimation of Peak Wind Effects on Structures." *Journal of Structural Engineering*, 139(3), 462-471.

Yeo, D. and Simiu, E. (2011). "High-Rise Reinforced Concrete Structures: Database-Assisted Design for Wind." *Journal of Structural Engineering*, 137(11), 1340-1349.

Appendix 1. Demand-to-Capacity Indexes for Steel Structures

The demand-to-capacity index (DCI) is the left-hand side of the design interaction equation and is a measure of the degree to which structural members are designed adequately for strength (Simiu 2011). The final design for strength is achieved when the DCIs of members are as close as possible to unity, to within specified serviceability constraints. The available strengths in this report are based on the AISC 360-10 (ANSI/AISC 2010a), and they depend on the cross-sectional shapes and types of member (i.e., column, beam, or bracing).

A. Members subjected to flexure and axial forces (B_{ij}^{PM})

$$\text{When } \frac{P_r}{\phi P_n} \geq 0.2, \qquad \frac{P_r}{\phi P_n} + \frac{8}{9} \cdot \left(\frac{M_{rx}}{\phi M_{nx}} + \frac{M_{ry}}{\phi M_{ny}} \right) \leq 1.0 \tag{A1}$$

$$\text{When } \frac{P_r}{\phi P_n} < 0.2, \qquad \frac{P_r}{2 \cdot \phi P_n} + \left(\frac{M_{rx}}{\phi M_{nx}} + \frac{M_{ry}}{\phi M_{ny}} \right) \leq 1.0 \tag{A2}$$

B. Members subjected to shear (B_{ij}^{V})

$$\frac{V_r}{\phi V_n} \leq 1.0 \tag{A3}$$

where P_r is the required axial strength using LRFD load combinations; P_n is the design tensile or compressive strength; M_{rx} is the required flexural strength about the strong axis using the LRFD load combinations; M_{ry} is the required flexural strength about the weak-axis using the LRFD load combinations; M_{nx} is the available flexural strength about the x-axis; M_{ny} is the available flexural strength about the y-axis; V_r is the required shear strength using the LRFD load combinations; V_n is the design shear strength; T_r is the required torsional strength using the LRFD load combinations; T_n is the design torsional strength; ϕ is the resistance factor for each type of strength.

C. HSS members subjected to combined torsion, shear, flexure, and axial force (B_{ij}^{PMVT})

When the required torsional strength is less than or equal to 20 % of the available torsional strength, the interaction of torsion, shear, flexure and/or axial force for HSS (Hollowed Structural Section) shall be determined by the Equation (A1) or (A2) and the torsional effects shall be neglected. When the required torsional strength exceeds 20% of the available torsional strength, the interaction of torsion, shear, flexure and/or axial force shall be limited, at the point of consideration, by

$$\left(\frac{P_r}{\phi P_n} + \frac{M_{rx}}{\phi M_{nx}} + \frac{M_{ry}}{\phi M_{ny}} \right) + \left(\frac{V_r}{\phi V_n} + \frac{T_r}{\phi T_n} \right)^2 \leq 1.0 \tag{A4}$$

Appendix 2. Global responses: Inter-story drift and Acceleration

The time-series of the inter-story drift ratios at i^{th} story, $d_{i,x}(t)$ and $d_{i,y}(t)$, corresponding to the x and y axis, are

$$d_{i,x}(t) = \frac{[x_i(t) - D_{i,y}\theta_i(t)] - [x_{i-1}(t) - D_{i-1,y}\theta_{i-1}(t)]}{h_i} \tag{A5}$$

$$d_{i,y}(t) = \frac{[y_i(t) + D_{i,x}\theta_i(t)] - [y_{i-1}(t) + D_{i-1,x}\theta_{i-1}(t)]}{h_i} \tag{A6}$$

where $x_i(t)$, $y_i(t)$, and $\theta_i(t)$ are the displacements and rotation at the mass center of the i^{th} floor, $D_{i,x}$ and $D_{i,y}$ are distances along the x and y axes from the mass center of the i^{th} floor to the point of interest on that floor, and h_i is the i^{th} story height between mass centers of the i^{th} and the $(i\text{-}1)^{th}$ floor.

The time-series of the resultant accelerations at the i^{th} floor, $a_{i,r}(t)$ is expressed as:

$$a_{i,r}(t) = \sqrt{[\ddot{x}_i(t) - D_{i,y}\ddot{\theta}_i(t)]^2 + [\ddot{y}_i(t) + D_{i,x}\ddot{\theta}_i(t)]^2} \tag{A7}$$

where accelerations $\ddot{x}_i(t)$, $\ddot{y}_i(t)$, and $\ddot{\theta}_i(t)$ of the mass center at the top floor pertain to the x, y, and θ (i.e., rotational) axes, and $D_{i,x}$ and $D_{i,y}$ are the distances along the x and y axes from the mass center to the point of interest on the i^{th} floor.

Appendix 3. Change log

<u>*Revision 1 – March 7, 2017*</u>

▪ The influence coefficient matrix for the second-order analysis is calculated from the softened stiffness matrix ($K-K_G$). The results influenced by the modified matrix are revised in the publication including figures and tables:

- Figure 11 (Response databases of B_{ij}^{PM} and B_{ij}^{V})
- Figure 12 and 13 (2^{nd} order effect ratios depending on member types and wind speeds)
- Table 4 and 5 (Peak DCIs for two load combinations and second-order effects)

▪ Revised the peak inter-story drifts with respect to wind directions (Figure 15).